UPPSALA
UNIVERSITET

UPTEC F 21010
Examensarbete 30 hp
Januari 2021

Positioning Electric Field Sensors in the Marine Environment Using Passage Data

Maria Langkilde

Civilingenjörsprogrammet i teknisk fysik

UPPSALA
UNIVERSITET

Positioning Electric Field Sensors in the Marine Environment using Passage Data

Maria Langkilde

Abstract

When underwater sensors are being deployed there is always some uncertainty about the actual position of the sensors. The most common way of determine the sensors position is the use of hydro-acoustic methods. However, for electric field sensors the most favourable would be to use the sensor system itself. The first question being answered in this report is whether it is possible to position electric field sensors with the sensor system itself, and the answer is yes. An algorithm has been developed which calculates the relative position of the sensors based on data measured by the sensors when a dipole passes the sensor group. The algorithm extracts zero crossings of the z-components of the electric field measured by each sensor from the data, which are converted to moments in time, multiplied by the speed and course of the vessel and finally calculated into relative position vectors between the sensors using vector algebra. The result of the predicted relative position is within 0.2 m from the sensors' actual position, which answers the second question about how accurate the method is. However, the error estimation is within a couple of centimetres indicating that there are other sources of error than speed and course. The third question being answered is whether the method is better than acoustic methods, and the answer is no. Nonetheless, the methods are within the same order of magnitude. In conclusion, the method has acceptable performance, especially considering the fact that it can determine the position of the sensors with the sensor system itself which could be significant.

Teknisk-naturvetenskapliga fakulteten

Uppsala universitet, Uppsala

Handledare: Ulf Jordan Ämnesgranskare: Anders Rydberg

Examinator: Tomas Nyberg

ACKNOWLEDGEMENTS

First and foremost I would like to thank my supervisor Ulf Jordan for his outstanding guidance throughout this work. Your pedagogical way of describing everything between heaven and earth, in combination with your passion for science, has inspired me deeply. With you as my supervisor I have learned a lot, especially thanks to your structured way of working and ability to give constructive feedback. It has been a true pleasure working with you.

Further I would like to thank the Swedish Defence Research Agency (FOI) for giving me the opportunity to write my master thesis at the institution on this very interesting topic. Not to forget - many thanks to all employees at the underwater research group at FOI for invaluable support and great company during coffee breaks.

I would also like to thank my subject reviewer Anders Rydberg for reading my master thesis with a fresh pair of eyes and making sure that my work has been conducted within the framework of the subject.

Last but not least, I would like to express my gratitude to my friend Erica Svensson, for her support both during the thesis work and during five fantastic years at Uppsala University together, filled with laughter and great friendship.

POPULÄRVETENSKAPLIG SAMMANFATTNING

Elektromagnetiska undervattenssensorer används för att detektera fartyg och andra undervattensfarkoster, samt för att ta reda på hur naturen ser ut och vilka egenskaper den omgivande miljön har genom att mäta elektriska och magnetiska fält i vattnet. Vid utplacering av undervattenssensorer finns det alltid en viss osäkerhet kring sensorernas faktiska position, eftersom det inte går att se om sensorerna står rätt placerade på samma sätt som det gör på land. För att få korrekt data från sensorerna är det dock viktigt att den faktiska positionen fastställs. Detta görs med hjälp av ett positioneringssystem, ofta baserat på hydroakustisk vågutbredning. För elektriska fältsensorer skulle det vara fördelaktigt att istället använda sensorsystemet självt för att fastställa positionen och på så sätt inte vara beroende av ett externt hydroakustiskt sensorsystem. Ett externt system bidrar till ökad komplexitet i mätuppställningen och kan vara en källa till störningar. Frågorna som har tagits upp i denna rapport är huruvida det är möjligt att positionera en grupp elektriska fältsensorer med sensorsystemet självt, och om det är möjligt, hur noggranna de förutsedda positionerna är? Kan metoden möjligtvis vara bättre än hydroakustiska metoder?

Svaret på den första frågan är ja, det går att positionera en grupp elektriska fältsensorer med sensorsystemet självt. För att lyckas med det har en algoritm utvecklats som beräknar den relativa positionen mellan sensorerna i sensorgruppen med hjälp av data insamlat av sensorerna själva då en dipol passerar över dem, samt en feluppskattning av resultatet baserat på båtens kurs och fart då det är svårt att veta exakt hur fort båten färdas och i exakt vilken riktning.

Algoritmen har testats på data från en sensorgrupp bestående av fem sensorer fastmonterade på en balk på ca 5 m avstånd från varandra, vilket gör att sensorernas faktiska position i det fallet är känd. Det gör det lätt att jämföra den beräknade positionen av sensorerna från algoritmen med den faktiska positionen av sensorerna. Resultatet av de beräknade positionerna ligger inom 0.2 m från deras faktiska position, medan den beräknade feluppskattningen är inom ett antal centimeter.

Noggrannheten på den förutsedda positionen hos sensorerna är acceptabel, vilket också är svaret på fråga två, men eftersom feluppskattningen är lägre än felet som den förutsedda positionen ger tyder det på att det finns andra felkällor än båtens fart och kurs. Möjliga källor som kan ge upphov till fel är att dipolen som färdas över sensorgruppen inte är horisontell i vattnet, att dipolens ena punktkälla

har förskjutits i sidled längs kurslinjen, att sensorerna lutar samt att havsbotten sluttar.

Svaret på om metoden är bättre än hydroakustiska metoder är nej, med det sagt är den inte mycket sämre heller. Hydroakustiska metoder kan ange en förutsedd position inom ett antal centimeter upp till ett antal decimeter från sensors faktiska position vilket gör att metodernas noggrannhet är av samma storleksordning. Även om hydroakustiska metoder ger ett något bättre resultat så är det till stor fördel att kunna använda sensorsystemet självt för att positionera elektriska fältsensorer och inte vara i behov av att använda ett externt system.

Sammanfattningsvis så har metoden acceptabel prestanda för att positionera elektriska undervattenssensorer.

CONTENTS

1 INTRODUCTION

1.1 PURPOSE AND APPLICATION

Electromagnetic underwater sensors are mainly used in three applications; to measure electric and magnetic signatures of vessels and other underwater vehicles, to measure electric and magnetic background fields to find out what the environment looks like and also to measure electric and magnetic fields obtained from natural or artificial sources to estimate the characteristics of the surrounding environment. When deploying underwater sensors, there is always some uncertainty about the actual position of the sensors. Depending on what the data from the sensors will be used for, there are different requirements for accuracy in positioning. These can be both requirements for absolute position or relative position within a group of several sensors.

Existing systems for underwater positioning are based on hydro-acoustic wave propagation and ditto sensors. For an electromagnetic sensor system without acoustic sensors, it is desirable to be able to use electromagnetic methods in order to determine its relative position with the system itself. The main advantage of determining the position with the sensor system itself is that an external system is not needed. An external system contributes to an increased complexity in the measurement setup and could be a source of disturbance.

1.2 PROJECT DESCRIPTION

The goal of this project is to investigate possible methods for positioning of electric field underwater sensors. The investigation includes a mathematical estimate of the accuracy that can be achieved with the proposed method, as well as a comparison with the performance of existing hydro-acoustic methods. The questions that are answered at the end of this thesis are the following:

- Is it possible to position electric field underwater sensors with the sensor system itself?
- How accurate is the estimated position of the sensors?
- Is this method of estimation better than hydro-acoustic methods?

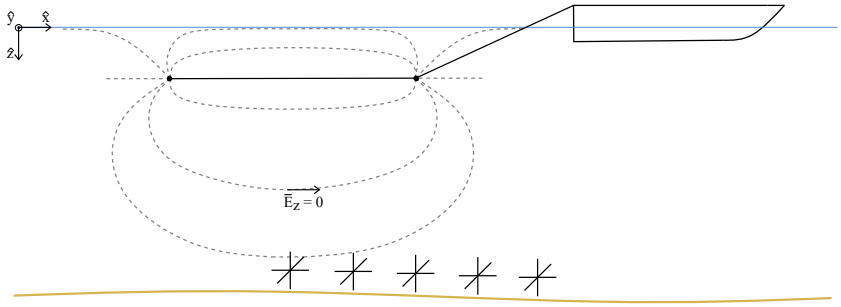

Figure 1: A dipole towed after a boat over a group of sensors which detects the electric field from the dipole due to carbon fibre electrodes that measures electric potential in x-, y- and z-direction. When the dipole is passing over a sensor there is a zero crossing among the z-components of the electric field detected by that sensor.

1.2.1 *Overview*

In this project a sensor group of five electric field sensors is used both for measured data and simulated data. The sensors of interest are triaxial sensors with one pair of carbon fibre electrodes mounted on each axis, making three pairs of electrodes in total. Each electrode pair measures electric potential and is therefore able to recognize change in the electric field in three directions. The axes of each sensor coincides with a global coordinate system making those directions the x-direction, y-direction and z-direction in a coordinate system. When a dipole runs over the sensor group the dipole generates an electric field which consequently is detected by the sensors and their electrode pairs. The z-direction in the global coordinate system points from the surface vertically down revealing that where there is a zero crossing among the z-components of the electric field detected by a sensor there is a passage of the dipole over that sensor in that moment. See Figure 1 for illustration. However, the dipole did not necessarily pass right above the sensor but somewhere close. The zero crossings only indicates a front of where each sensor is located, see Figure 2, further a position vector from every sensor to a reference point is calculated with the help of vector algebra. Sensor 2 is arbitrarily used throughout this project as reference point.

Ultimately, the relative position of the sensors in the sensor group can be calculated by extracting the data points where there is a zero crossing among the z-components of the electric field for each sensor and converting these data points to moments in time. Multiplying these by the speed and course of the vessel in question makes it possible to calculate the relative position vector to each sensor, obtaining a relative distance.

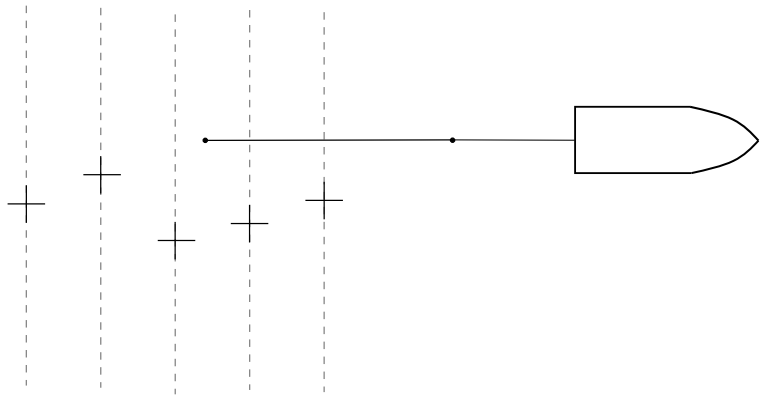

Figure 2: The dipole does not have to pass right above each sensor. The zero crossings among the z-components of the electric field only indicates a front where each sensor can be located, further a position vector from every sensor to a reference sensor needs to be calculated.

1.3 LIMITATIONS

However, there are limitations that probably will affect the result when the above stated calculations are made, like the fact that the dipole which runs over the sensor group might not be horizontal, that one of the sources of the dipole are offset sideways, that the sensors might be tilted or that the seabed is sloping. Both an uneven dipole, a tilted sensor and a sloping seabed affects the electric field by displacement. Throughout Section 2.2 the limitations are further investigated.

2 THEORY AND BACKGROUND

2.1 ELECTROMAGNETIC FIELD THEORY

Electromagnetic phenomena are described by electromagnetic field theory. A comprehensive introduction to the subject may be obtained from any university level textbook, see for example [3] and [14]. Below follows a short summary of the theory needed for this work.

2.1.1 *Maxwell's equations*

Electromagnetic field theory is described by Maxwell's equations, originally established by James Clerk Maxwell in 1861, later reformulated by Oliver Heaviside with modern vector designations into four partial differential equations, Equation 1 – Equation 4.

$$\nabla \cdot \bar{D} = \rho \tag{1}$$

The first of Maxwell's equations, Equation 1, states that electric fields are caused by electric charges, and is therefore not prone to exist without electric charges. Positive charges have electric fields that go outwards from the charge and negative charges have electric fields that go inwards to the charge. That means that two charges of the same sign repel each other and two charges with opposite sign attract each other. The divergence, $\nabla\cdot$, is a measure of the outward flux of the vector field from a specific point, $\bar{D}$ is the electric flux density which is the the electric field $\bar{E}$ multiplied with the static permittivity ϵ, and ρ is the charge density.

$$\nabla \cdot \bar{B} = 0 \tag{2}$$

The second of Maxwell's equations, Equation 2, further describes with Gauss law for magnetic fields how there are no isolated charges, also called monopoles, for magnetic fields. This means magnetic fields never diverge away from one point as electric fields do, described in Equation 1, instead magnetic field lines are always closed. Consequently the surface integral of a magnetic field over a closed surface equals zero. The divergence, $\nabla\cdot$, is again a measure of the outward flux of the vector field from a specific point and $\bar{B}$ is the magnetic flux

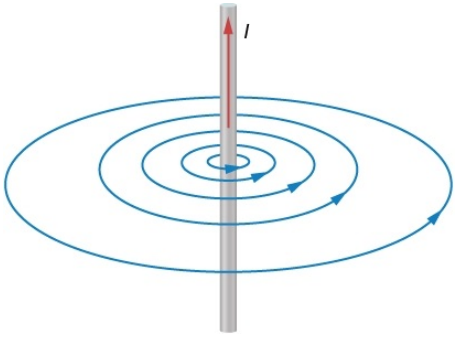

Figure 3: The magnetic field, $\bar{B}$, that arise around an electric conductor when an electric current, I, is induced in the conductor.

density which is the magnetic field $\bar{H}$ multiplied with the permeability μ.

$$\nabla \times \bar{E} = -\frac{\partial \bar{B}}{\partial t} \tag{3}$$

The third of Maxwell's equations, Equation 3, also known as Faraday's law of induction, defines how electric fields emerges from variations in the magnetic field. If an electrical conductor moves through a magnetic field, or if the surrounding magnetic field is changed, an electric current is induced in the electric conductor, due to the voltage that arises. The curl, $\nabla\times$, describes the rotation of a vector field in a three-dimensional Euclidean space, $\bar{E}$ is the electric field and $\bar{B}$ is the magnetic flux density.

$$\nabla \times \bar{H} = \bar{J} + \frac{\partial \bar{D}}{\partial t} \tag{4}$$

The fourth of Maxwell's equations, Equation 4, also known as Ampère's law with Maxwell's corrections, declares in contrary how magnetic fields emerge from variations in the electric field. If an electric current flows in an electric conductor a magnetic field arises around the conductor as in Figure 3. The curl, $\nabla\times$, again describes the rotation of a vector field in a three-dimensional Euclidean space, while $\bar{J}$ is the charge density at a given location.

For a linear isotropic medium, Ohm's model takes the form $\bar{J} = \sigma\bar{E}$, where σ is the electric conductivity of the medium. Assuming harmonic time dependence $\frac{\partial \bar{D}}{\partial t} = j\omega\epsilon\bar{E}$, where $\omega = 2\pi f$ is the angular frequency. In brackish water the conductivity σ is approximately 1 S/m. For low frequencies, i.e. $\omega\epsilon \ll \sigma$, the conduction current $\bar{J}$ will completely dominate over the displacement current $\frac{\partial \bar{D}}{\partial t}$ in the right hand side of Equation 4. This is the case when, for example, the frequency $f < 1$ kHz in brackish water.

2.1.2 *Electric dipole in vacuum*

An electric dipole consists of two electric charges of equal magnitude with opposite sign at a small distance from each other. Characteristic for the dipole is its dipole moment, which is a measurement of the polarity of the dipole as a vector quantity. The direction of the dipole moment points in the direction from the negative charge towards the positive charge, and the magnitude, p, is calculated by multiplying the strength of each charge, Q, with the distance between the charges, d, as in Equation 5.

$$\bar{p} = Q\bar{d} \tag{5}$$

The two charges of opposite sign causes an electric field that is given by Equation 6 in vacuum, where ϵ_0 is the vacuum permittivity, $\bar{r}$ is the vector from the centre of the dipole to the field point and $\bar{p}$ is the dipole moment.

$$\bar{E} = \frac{1}{4\pi\epsilon_0 r^3}\left[3\frac{\bar{r}\cdot\bar{p}}{r^2}\bar{r} - \bar{p}\right] \tag{6}$$

2.2 MEASUREMENT METHODS AND CALCULATION MODELS

In the setup there are a couple of measurement methods and calculation models that are of great importance in order for the measurement to work and turn out as desired. In this section the most important ones are presented.

2.2.1 *Environmental impact on the electric field from a dipole in conducting medium*

The environment is in the general case a three dimensional structure with a distribution of conductivity σ. However, due to the stratification, a good local model of the environment can be obtained by approximation with horizontal layers. For example an environment can be divided into one layer of air, one layer of water and one layer of seabed which in turn consists of several layers. If a dipole moves through water the electric field emitted from the dipole will be affected by the layer of air and the layer of seabed since air, water and sand has different conductivity σ. Accordingly it is of interest to calculate the total electric field in any point $\bar{r}$, $\bar{E}(\bar{r})$, in the environment to map how the electric field changes depending on the surrounding layers. Figure 4 illustrates the environment where $\bar{r}_s$ is the position of a source representing a dipole and $\bar{r}$ is any point in the environment.

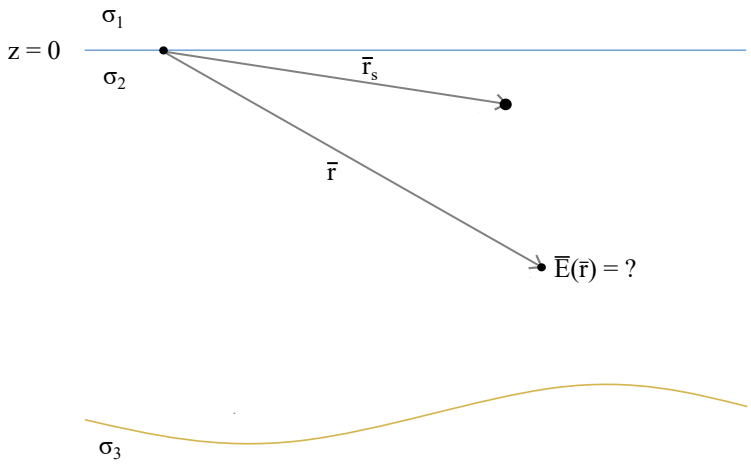

Figure 4: A source at position $\bar{r}_s$ and a point $\bar{r}$ located in water with one layer of air above the water with conductivity $\sigma_1 = 0$ and one layer of seabed beneath the water with conductivity σ_3. The electric field in point $\bar{r}$, $\bar{E}(\bar{r})$, and how it is affected by the layers of air and seabed is of interest.

2.2.1.1 *Whole space*

To be able to calculate this the problem is divided into sub parts. Initially the electric field $\bar{E}$ for one point $\bar{r} = (x, y, z)$ is calculated in a whole space denoting that there are no layers. This is done from Ohm's model in Equation 7, which is possible if the current density at a given location $\bar{J}$ and the conductivity σ is known.

$$\bar{J} = \sigma \bar{E} \tag{7}$$

Therefore, to begin with $\bar{J}$ is calculated. The magnitude of $\bar{J}$ equals the current density from one point source with current I_s that flows out evenly from the point source at $\bar{r}_s = (x_s, y_s, z_s)$, see Figure 5, and is written as

$$|\bar{J}| = \frac{I_s}{4\pi |\bar{R}_s|^2}. \tag{8}$$

The direction of $\bar{J}$ in point $\bar{r}$ is the same as the direction between point $\bar{r}$ and the point source $\bar{r}_s$, $\hat{R}_s = \frac{\bar{R}_s}{|\bar{R}_s|}$. With vector algebra $\bar{R}_s$ can be written as $\bar{R}_s = \bar{r} - \bar{r}_s$. Multiplying $\hat{R}_s$ with $|\bar{J}|$ gives all together an expression for $\bar{J}(\bar{r})$:

$$\bar{J}(\bar{r}) = \frac{I_s}{4\pi} \frac{(\bar{r} - \bar{r}_s)}{|\bar{r} - \bar{r}_s|^3}. \tag{9}$$

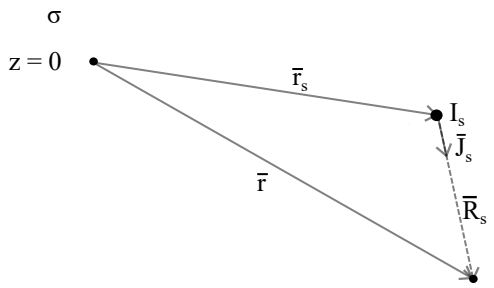

Figure 5: A current source I_s at position $\bar{r}_s$ and a point $\bar{r}$ located in a whole space, meaning that the conductivity σ is the same in the entire space.

Further, dividing $\bar{J}$ by the conductivity σ gives the electric field $\bar{E}$:

$$\bar{E} = \frac{I_s}{4\pi\sigma}\frac{(\bar{r}-\bar{r}_s)}{|\bar{r}-\bar{r}_s|^3}. \tag{10}$$

When the electric field $\bar{E}$ is found it is of interest to investigate the curl and the divergence of $\bar{E}$. The curl is calculated by Equation 11.

$$\nabla \times \bar{E} = (\frac{\partial E_z}{\partial y} - \frac{\partial E_y}{\partial z})\hat{x} - (\frac{\partial E_z}{\partial x} - \frac{\partial E_x}{\partial z})\hat{y} + (\frac{\partial E_y}{\partial x} - \frac{\partial E_x}{\partial y})\hat{z} \tag{11}$$

Evaluating Equation 11 gives that the curl of $\bar{E}$ equals to zero since the terms in each direction cancel each other out. This means that the electric field is stationary. To continue, the divergence is calculated by Equation 12.

$$\nabla \cdot \bar{E} = \frac{\partial E_x}{\partial x} + \frac{\partial E_y}{\partial y} + \frac{\partial E_z}{\partial z} \tag{12}$$

Substituting the expression for $\bar{E}$ from Equation 10 in Equation 12 gives equation Equation 13, which results in that the divergence of the electric field equals to zero in all points except point $\bar{r}_s = (x_s, y_s, z_s)$. Concluded the environment is source-free apart from the point source.

$$\nabla \cdot \bar{E} = \frac{I_s}{4\pi\sigma}\frac{1}{((x-x_s)^2+(y-y_s)^2+(z-z_s)^2)^{-\frac{3}{2}}}(3-3) = 0 \tag{13}$$

All together, the curl and the divergence of $\bar{E}$ shows that Equation 10 gives the stationary electric field for whole space consisting of no other charges than the point source.

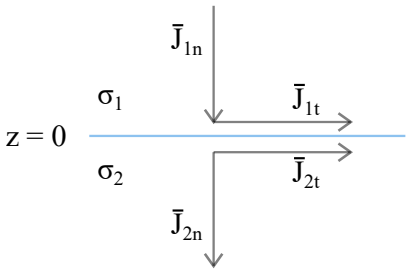

Figure 6: The normal and tangential components at the boundary in the first and second domain of the half-space.

2.2.1.2 *Half space – mirror solution*

Next step is to calculate the stationary electric field for half space, denoting that there are two layers, which is done by a mirror solution. In order to use the mirror solution it is of importance to look at the boundary conditions, more precisely the normal and tangential components at the boundary in the first and the second domain of the half-space, see Figure 6. The relation between the domains for the normal components are

$$\bar{J}_{2n} = \bar{J}_{1n}, \tag{14}$$

and for tangential components

$$\frac{\bar{J}_{2t}}{\sigma_2} = \frac{\bar{J}_{1t}}{\sigma_1}. \tag{15}$$

The mirror solution used in half-space when there are only two layers consists of three steps.

I. The first step is to calculate the charge density at any point, $\bar{J}(\bar{r})$, when that point $\bar{r}$ is within the same domain as the source at $\bar{r}_s$, see Figure 7. With the intention to do so the source at $\bar{r}_s$ is mirrored into the opposite domain so that $z_m = -z_s$ in order to not get a trivial solution. When $\bar{r}_s$ is mirrored into the other domain the boundary can be ignored and the whole space is assumed to have same conductivity as the domain where point $\bar{r}$ is located, in this case σ_2. Further the current density at point $\bar{r}$ in the second domain, $\bar{J}_2(\bar{r})$, is calculated in the same way as Equation 9 except the contribution from two point sources in this case, at $\bar{r}_s$ and $\bar{r}_m = (x_m, y_m, z_m)$. The result divided into x-, y- and z-components, is represented by Equation 16 – Equation 18.

$$\bar{J}_{2x} = \frac{I_s}{4\pi} \frac{(x - x_s)}{|\bar{r} - \bar{r}_s|^3} \hat{x} + \frac{I_m}{4\pi} \frac{(x - x_m)}{|\bar{r} - \bar{r}_m|^3} \hat{x} \tag{16}$$

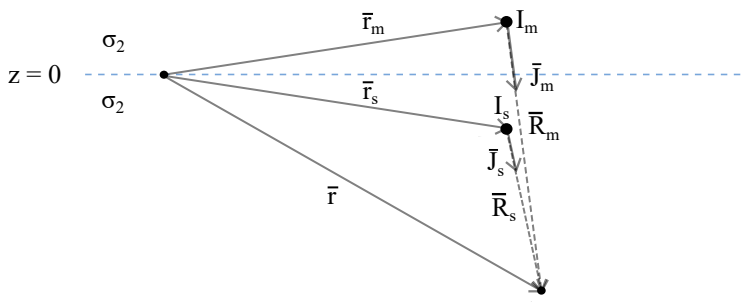

Figure 7: The mirror solution for any point $\bar{r}$ located in the same domain as the source at $\bar{r}_s$ which is mirrored into the other domain creating a mirrored source at $\bar{r}_m$. When the source is mirrored into the other domain the boundary can be ignored and the conductivity is assumed to be the same as in the domain where point $\bar{r}$ is located, in this case σ_2, in the entire space.

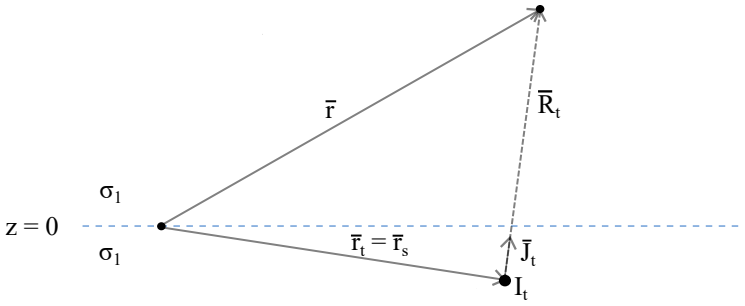

Figure 8: The mirror solution for any point $\bar{r}$ located in the opposite domain from the source $\bar{r}_s$ which makes the mirrored point $\bar{r}_t$ appear in the same point as the source $\bar{r}_s$. The boundary can be ignored and the conductivity is assumed to be the same as in the domain where $\bar{r}$ is located, in this case σ_1, in the entire space.

$$\bar{J}_{2y} = \frac{I_s}{4\pi}\frac{(y-y_s)}{|\bar{r}-\bar{r}_s|^3}\hat{y} + \frac{I_m}{4\pi}\frac{(y-y_m)}{|\bar{r}-\bar{r}_m|^3}\hat{y} \tag{17}$$

$$\bar{J}_{2z} = \frac{I_s}{4\pi}\frac{(z-z_s)}{|\bar{r}-\bar{r}_s|^3}\hat{z} + \frac{I_m}{4\pi}\frac{(z-z_m)}{|\bar{r}-\bar{r}_m|^3}\hat{z} \tag{18}$$

II. The second step of the mirror solution for half-space is to calculate the charge density at any point, $\bar{J}(\bar{r})$, when that point $\bar{r}$ is located in the opposite domain as the source at $\bar{r}_s$. The source is now assumed to be located at $\bar{r}_t = (x_t, y_t, z_t)$. To avoid a trivial solution in this case, $z_t = z_s$ which means that z_t is located in the same point as z_s, see Figure 8. Also here the boundary can be ignored and the whole space is assumed to consists of the conductivity that exists in the same domain as point $\bar{r}$, in this case σ_1. The charge density at point $\bar{r}$ located in the first domain, $\bar{J}_1(\bar{r})$, is also calculated as Equation 9. Divided into x-, y- and z-components it is represented by Equation 19 – Equation 21.

$$\bar{J}_{1x} = \frac{I_t}{4\pi}\frac{(x-x_t)}{|\bar{r}-\bar{r}_t|^3}\hat{x} \tag{19}$$

$$\bar{J}_{1y} = \frac{I_t}{4\pi}\frac{(y-y_t)}{|\bar{r}-\bar{r}_t|^3}\hat{y} \tag{20}$$

$$\bar{J}_{1z} = \frac{I_t}{4\pi}\frac{(z-z_t)}{|\bar{r}-\bar{r}_t|^3}\hat{z} \tag{21}$$

III. The third step of the mirror solution is to match the calculated results of the current density in any point, $\bar{J}(\bar{r})$, on the boundary $z = 0$ from both the case when $\bar{r}$ is located in the same domain as the source and the case when it is located in the opposite domain. It is known that $z_s = -z_m = z_t$ and according to symmetry the mirrored source can not move from the source in x- and y-direction which gives that $x_s = x_m = x_t$ and $y_s = y_m = y_t$. The coordinate system is located so that the z-axis points from the surface down and the x- and y-axis points along the surface. This means that the z-components represent the normal components and the x- and y-components represent the tangential components. Inserting Equation 18 and Equation 21 into Equation 14 with $z_s = -z_m = z_t$ gives Equation 22.

$$I_m = I_s - I_t \tag{22}$$

Continuously inserting Equation 16, Equation 17, Equation 19 and Equation 20 into Equation 15 with $x_s = x_m = x_t$ and $y_s = y_m = y_t$ gives Equation 23.

$$I_t = \frac{\sigma_1}{\sigma_2}(I_s + I_m) \tag{23}$$

This provides two equations, Equation 22 and Equation 23, as well as two unknown variables, I_m and I_t, since I_s is known from assumption. Inserting Equation 23 into Equation 22 gives I_m as Equation 24.

$$I_m = I_s\left(\frac{\sigma_2 - \sigma_1}{\sigma_2 + \sigma_1}\right) \tag{24}$$

Inserting Equation 24 into Equation 23 gives I_t as Equation 25.

$$I_t = I_s\left(\frac{2\sigma_1}{\sigma_2 + \sigma_1}\right) \tag{25}$$

All together this gives an expression for the current density in any point in the half-space considering that I_m and I_t is inserted into Equation 16 – Equation 21. An expression for the electric field $\bar{E}$ is obtained by dividing the charge density in any point, $\bar{J}$, by σ for each domain respectively as Equation 26.

$$\bar{E} = \begin{cases} \frac{I_s}{4\pi\sigma_2}\frac{\bar{r}-\bar{r}_s}{|\bar{r}-\bar{r}_s|^3} + \frac{I_m}{4\pi\sigma_2}\frac{\bar{r}-\bar{r}_m}{|\bar{r}-\bar{r}_m|^3}, & z \geqslant 0 \\ \frac{I_t}{4\pi\sigma_1}\frac{\bar{r}-\bar{r}_t}{|\bar{r}-\bar{r}_t|^3}, & z \leqslant 0 \end{cases} \tag{26}$$

To avoid division by zero, if $\sigma_1 = 0$, insert the expression for I_t from Equation 25 into Equation 26 to get Equation 27.

$$\bar{E} = \begin{cases} \frac{I_s}{4\pi\sigma_2}\frac{\bar{r}-\bar{r}_s}{|\bar{r}-\bar{r}_s|^3} + \frac{I_m}{4\pi\sigma_2}\frac{\bar{r}-\bar{r}_m}{|\bar{r}-\bar{r}_m|^3}, & z \geqslant 0 \\ \frac{I_s}{4\pi}\frac{2}{\sigma_2+\sigma_1}\frac{\bar{r}-\bar{r}_t}{|\bar{r}-\bar{r}_t|^3}, & z \leqslant 0 \end{cases} \tag{27}$$

In order to get the total electric field in point $\bar{r}$, a super position of the electric fields from all point charges $\bar{r}_{si}$ is done as in Equation 28 for $z \geqslant 0$

$$\bar{E} = \sum_{i=1}^{N} \frac{I_{si}}{4\pi\sigma_2} \frac{\bar{r} - \bar{r}_{si}}{|\bar{r} - \bar{r}_{si}|^3} + \frac{I_{mi}}{4\pi\sigma_2} \frac{\bar{r} - \bar{r}_{mi}}{|\bar{r} - \bar{r}_{mi}|^3}, \qquad i = 1, \cdots, N \tag{28}$$

with I_{mi} calculated from I_{si} using Equation 24, and as Equation 29 for $z \leqslant 0$

$$\bar{E} = \sum_{i=1}^{N} \frac{I_{si}}{4\pi} \frac{2}{\sigma_2 + \sigma_1} \frac{\bar{r} - \bar{r}_{ti}}{|\bar{r} - \bar{r}_{ti}|^3}. \qquad i = 1, \cdots, N. \tag{29}$$

2.2.1.3 *Calculated field images*

To illustrate how the electric field is affected by the environment that consist of layers with various conductivity, field images of the electric field are calculated. First of all, a matrix for all points $\bar{r}$ that spans the room is created, with a selected number of linearly equally spaced data points in x-direction between $x_{min} = -20$ m and $x_{max} = 30$ m, a selected number of linearly equally spaced data points in y-direction between $y_{min} = -15$ m and $y_{max} = 15$ m as well as constant depth $z_0 = 10$ m in z-direction. The number of linearly equally spaced points are selected to 500 in x-direction and 300 in y-direction. Next, a function created to calculate the electric field in any point $\bar{r}$ based on the formulas in Section 2.2.1.1 and Section 2.2.1.2 is used, which further extracts the x-, y-, and z-components of the electric field and reshapes them to fit the number of data points in x- and y-direction. After that, the x-, y- and z-components of the electric field are plotted using 'imagesc' in Matlab which generates an image with scaled colours. Figure 9 shows these images for whole space, while Figure 10 shows them for half space. Note that the difference between whole and half space solutions is mainly in the quantitative magnitude of the field strength. The qualitative features such as locations of extrema and zero crossings remain the same.

2.2.2 *Two monopoles as an approximate dipole*

An approximate method in order to generate a current dipole is to place two monopoles of opposite sign close to each other. In this project two copper bars, that acts as electrodes, with a constant current I supplied to them, placed on a distance $d = 10$ m from each other generates an approximate dipole. This dipole is further attached to a boat that steers over the sensor group.

When the dipole is towed behind the boat the dipole might not be horizontal due to the towing force, resulting in different depths of the monopoles when the boat is moving forward. There is also a possibility that the monopoles are offset from the course line. Consequently

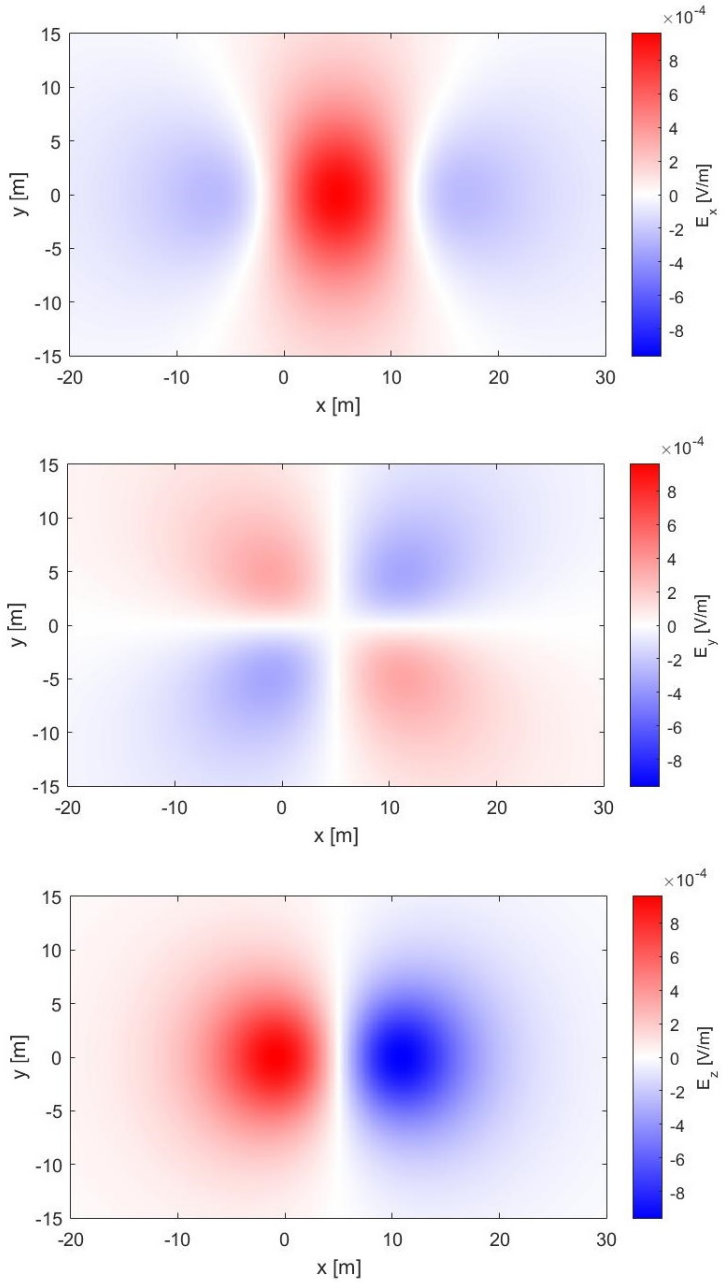

Figure 9: Plot of the x-components (top), y-components (centre) and z-components (bottom) of the electric field at depth $z = 10$ m when the sources of the dipole are static at position $\bar{r}_{s1} = [10 \quad 0 \quad 2]$ m with current $I_1 = -1$ A and $\bar{r}_{s2} = [0 \quad 0 \quad 2]$ m with current $I_2 = 1$ A, for whole space.

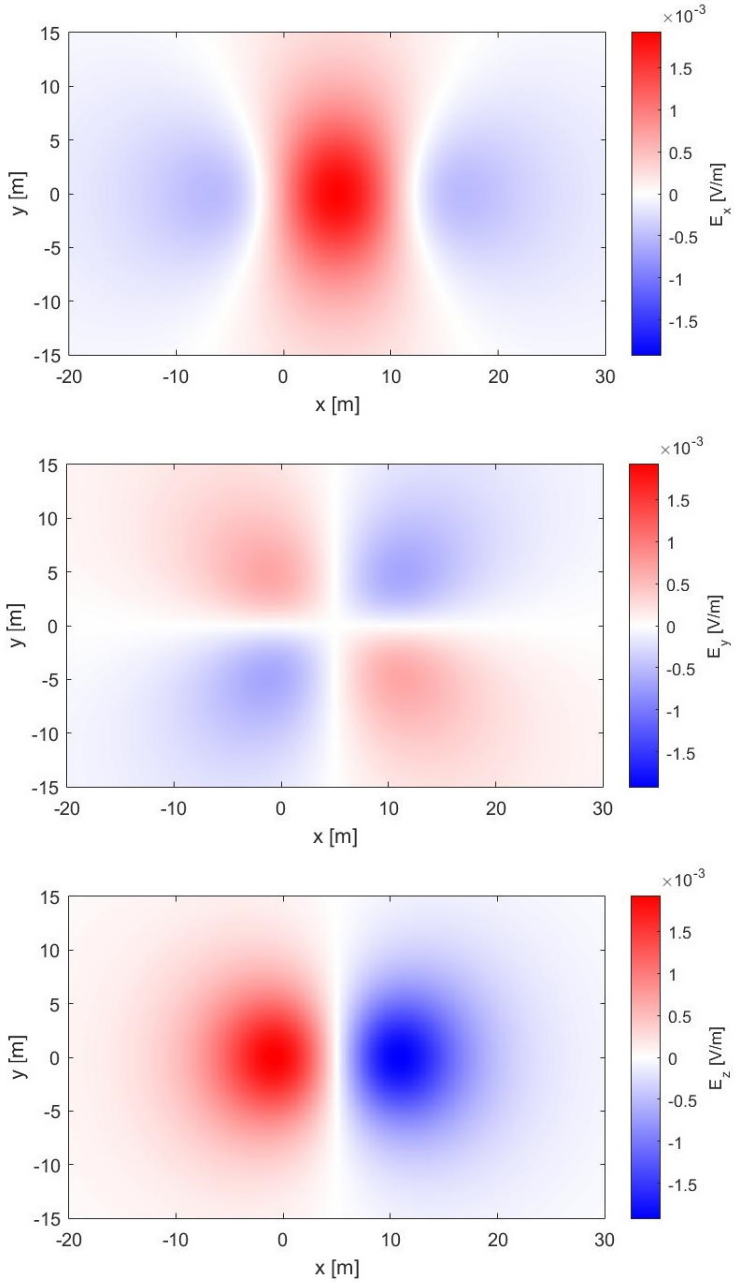

Figure 10: Plot of the x-components (top), y-components (centre) and z-components (bottom) of the electric field at depth $z = 10$ m when the sources of the dipole are static at position $\bar{r}_{s1} = [10 \quad 0 \quad 2]$ m with current $I_1 = -1$ A and $\bar{r}_{s2} = [0 \quad 0 \quad 2]$ m with current $I_2 = 1$ A, for half space.

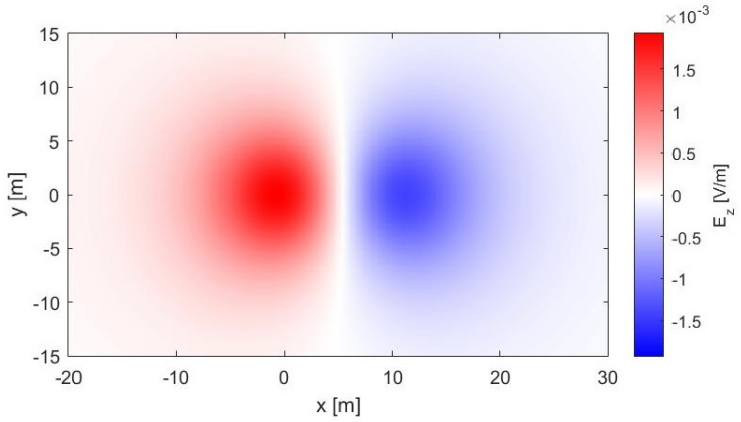

Figure 11: Plot of the z-components of the electric field E_z at depth $z = 10$ m when the sources of the dipole is static at position $\bar{r}_{s1} = [10 \quad 0 \quad 1]$ m with current $I_1 = -1$ A and $\bar{r}_{s2} = [0 \quad 0 \quad 2]$ m with current $I_2 = 1$ m, and therefore is non-horizontal, for whole space.

the vector components of the electric field will be affected and therefore it is of importance to investigate. With the aim to do that a data file is generated consisting of the x-, y- and z-components of the electric field emitted from the dipole at different time steps measured in five simulated sensors. By using this simulated data file it is possible to calculate how the electric field is affected by an uneven dipole without any other disturbances.

2.2.2.1 *Calculated field images of uneven dipole*

The field images in Figure 11 – Figure 13 show how the z-components of the electric field are affected by an uneven dipole. Observed from the field image in Figure 11 the zero crossings of the z-component of the electric field are curved towards smaller x-values at the edges when the dipole is non-horizontal. When the dipole on the other hand is uneven due to that the first source is offset sideways, in negative or positive y-direction, the zero crossings are shifted as in Figure 12 and Figure 13.

2.2.3 *Carbon fibre electrodes*

Carbon fibre electrodes can be used in electromagnetic sensors to measure electric fields in marine environments. Advantages of the electrodes are that they have low self noise as well as short stabilisation time before they are operational after deployment. The carbon fibres do also have the advantage of having a large surface to weight ratio at 0.5 m^2/g together with that they are inert in water. [4]

In order to measure x-, y- and z-components of the electric field triaxial carbon fibre sensors are used. The triaxial sensors has, as the

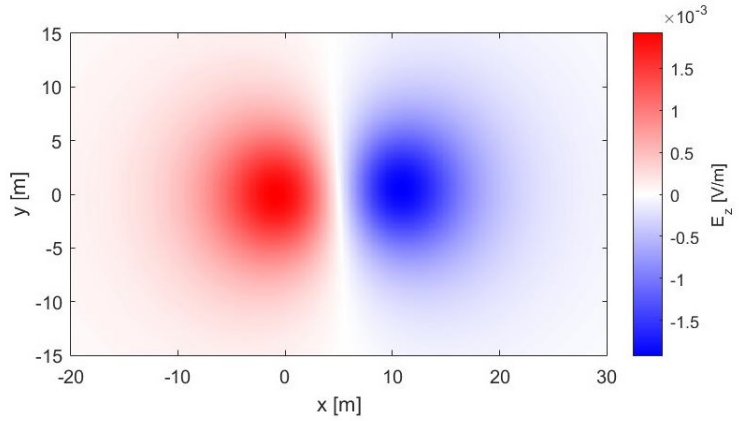

Figure 12: Plot of the z-components of the electric field E_z at depth $z = 10$ m when the sources of the dipole is static at position $\bar{r}_{s1} = [10 \quad 0.5 \quad 2]$ m with current $I_1 = -1$ m and $\bar{r}_{s2} = [0 \quad 0 \quad 2]$ m with current $I_2 = 1$ m for whole space.

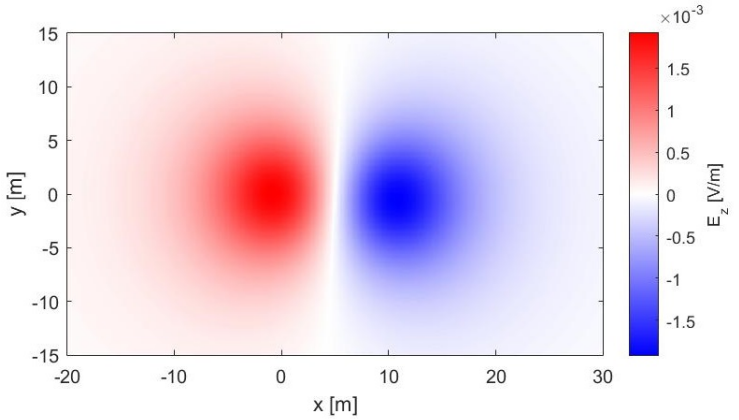

Figure 13: Plot of the z-components of the electric field E_z at depth $z = 10$ m when the sources of the dipole is static at position $\bar{r}_{s1} = [10 \quad -0.5 \quad 2]$ m with current $I_1 = -1$ m and $\bar{r}_{s2} = [0 \quad 0 \quad 2]$ m with current $I_2 = 1$ m for whole space.

Figure 14: Example of a three axis E-field sensor with carbon fibre electrodes mounted in pairs along the coordinate system axis. Photo courtesy of FOI.

name indicates, three axes where carbon fibre electrodes are mounted in pairs, as the construction shows in Figure 14. When the sensors are deployed at the bottom of the sea the three axes are placed so they coincides with a chosen global coordinate system which makes the sensor a coordinate system itself with one pair of carbon fibre electrodes at each coordinate axis. Every pair of carbon fibre electrodes measure electric potential. [4]

2.2.4 *Correctly aligned sensors*

It is of importance that the three axes of the sensors coincides with the global coordinate system so that the sensors are aligned correctly, which would not be the case if one of the sensors is tilted. To simulate a tilted sensor the electric field of that sensor is multiplied with a rotation matrix. The sensor and its coordinate system is able to rotate in three dimensions namely yaw, pitch and roll, also called vertical, transverse and longitudinal direction respectively. Therefore the total rotation matrix is the product of the rotation matrix for yaw, pitch and roll shown in Equation 30 where α, β and γ are the yaw, pitch and roll angles respectively, cf. Appendix B in reference [6].

$$R = \begin{bmatrix} 1 & 0 & 0 \\ 0 & \cos\gamma & \sin\gamma \\ 0 & -\sin\gamma & \cos\gamma \end{bmatrix} \begin{bmatrix} \cos\beta & 0 & -\sin\beta \\ 0 & 1 & 0 \\ \sin\beta & 0 & \cos\beta \end{bmatrix} \begin{bmatrix} \cos\alpha & \sin\alpha & 0 \\ -\sin\alpha & \cos\alpha & 0 \\ 0 & 0 & 1 \end{bmatrix} \tag{30}$$

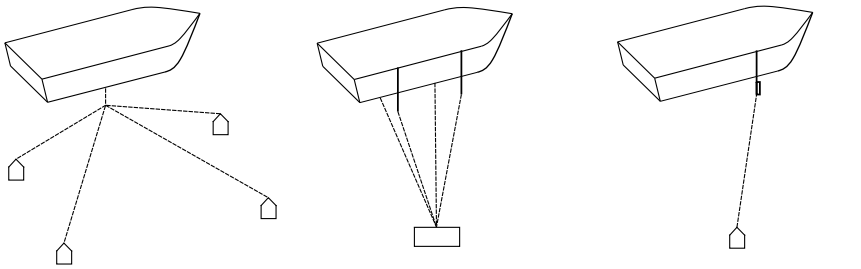

Figure 15: Three hydro-acoustic positioning methods widely used for underwater position determination, Long Baseline (LBL), Short Baseline (SBL) and Ultra Short Baseline (USBL) systems.

2.3 HYDRO-ACOUSTIC METHODS

In order to do a comparison with the performance of existing hydro-acoustic methods the following section will present the most common hydro-acoustic methods and their performance. Acoustic positioning systems are widely used for underwater position determination with the same purpose as the Global Positioning System (GPS) except it works well in water. Why GPS does not work well in water is due to the relatively high frequency radio waves GPS uses which becomes indistinct under water due to absorption. The three most common underwater acoustic positioning methods are Long Baseline (LBL) systems, Short Baseline (SBL) systems and Ultra Short Baseline (USBL) systems, see Figure 15. [5]

A LBL system uses a network of transponders located on the seabed together with an acoustic transducer mounted on a vessel. The transducer is usually active in LBL systems which means that the moment it detects a sound it pings, the transponders perceive the ping and confirms the round trip delay to the transducer by transmitting a response ping. The distance is calculated by measuring the time between transmission of the first signal and reception of the second in the transducer. [10] [2]

A SBL system on the other hand only needs to use three or more individual sonar transceivers mounted on a vessel, this means that the SBL system require no seafloor-mounted transponders. The system transmits from one transceiver, but receives on all of them which results in one distance measurement from the transceiver to the target and back, as well as a number of time differences. Both contributes to the calculation of the distance. [1] [2]

Lastly, an USBL system uses several transceivers tightly integrated on a pole mounted on a vessel as well as a transponder on the seafloor. A transceiver transmits a ping that is received by the transponder which in turn transmits a response ping back to all transceivers. In

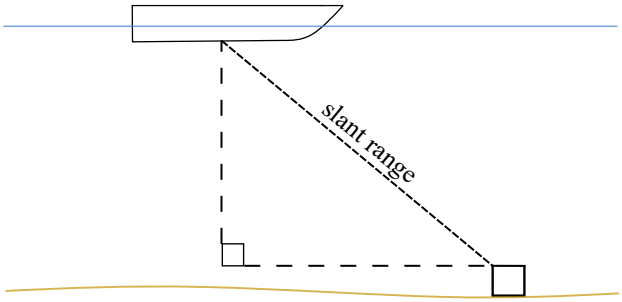

Figure 16: Illustration of slant range between a vessel and a target.

contrary to LBL and SBL systems, USBL systems measures the phase shift of the response ping within the transceivers and in that way calculates the distance to the target. [13] [5] [2]

The reason why the systems are called Long Baseline, Short Baseline and Ultra Short Baseline systems are due to the fact that the baseline distances are much longer for Long Baseline systems than for Short and Ultra Short Baseline systems. [5] The different systems operates at the following baseline lengths

- Long Baseline: 100 m to 6000 m+
- Short Baseline: 20 m to 50 m
- Ultra Short Baseline: <0.1 m. [13]

The longer the baseline the better the accuracy which in general makes a LBL system more accurate than a SBL and USBL system. [12] However there are other factors the accuracy depends on, for example LBL systems are independent of water depth but dependent on frequency while SBL systems are dependent of water depth as the accuracy is expressed in slant range which becomes greater with greater depth. [13] The accuracy may also depend on distance, geometry and sound propagation in water. Sound propagation in water is affected by the speed of the sound in water, absorption, reverberation, geometric scattering and sound deflection to mention some of the critical factors. [9] Accuracy for hydro-acoustic positioning systems are expressed either in meters or in slant range. Slant range is the distance between the vessel and the target as illustrated in Figure 16. According to commercial companies hydro-acoustic positioning systems have centimetric accuracy. For example the SHARPS SBL system which is used by The Woods Hole Oceanographic Institution

has a reported accuracy of 0.09 m. [2] Other examples are the USBL system from Advanced Navigation that have a position accuracy for acoustics of up to 0.25% of slant range [11], the acoustic underwater positioning and navigation system HiPAP from Kongsberg with a range detection accuracy of 0.02 m [7] as well as the Mini-Ranger 2 USBL system from Sonardyne with an accuracy of up to 1.3% of slant range. [8]

3 PROPOSED SOLUTION

To calculate the position of M number of sensors in a sensor system N number of runs over the system with a dipole will be performed. The position of each sensor k for each run i will be calculated. Important is that the dipole must travel in a straight line.

3.1 ALGORITHM

When the dipole passes one sensor k the z-component of the electric field is zero and therefore there is a zero crossing in the time series of the z-component during that run. By extracting the data points where there is a zero crossing it is known at which moment t_{ik} the dipole passes closest to sensor k in that run i. By selecting a reference point in space and establishing the time t_{i0} when the dipole passes that point, the relative time $\tau_{ik} = t_{ik} - t_{i0}$ can be calculated. If there is access to absolute positioning of the dipole, e.g. using satellite navigation, the reference position and corresponding time t_{i0} can be absolutely determined, and consequently also the absolute position of the sensors. In the opposite case, when the absolute position of the dipole is unknown, we may still obtain the relative position between the sensors, by designating one of them K as the reference point and taking $t_{i0} = t_{iK}$ from that sensor for run i. In the following we will assume that this is the case. The speed, v_i, and course, α_i, of the vessel, and therefore the speed and course of the dipole, can be extracted from meta data. The course is the angle measured between north (pointing in x-direction) and the direction of travel. Since both the relative time between the sensors as well as the speed and course of the dipole is known, the relative distance, s_{ik}, between the sensors can be calculated. A vector, $\bar{s}_{ik}$, is created with the length $s_{ik} = v_i\tau_{ik}$ and direction $(\cos\alpha_i, \sin\alpha_i, 0)$ as in Equation 31, see Figure 17.

$$\bar{s}_{ik} = v_i\tau_{ik}(\cos\alpha_i, \sin\alpha_i, 0) \tag{31}$$

However, the dipole might not pass straight over each sensor since the zero crossing indicates a front of where a sensor is located. Denoting that a position vector, $\bar{r}_k$, for each sensor relative to the reference point needs to be determined, see Figure 17. Assume that $\bar{r}_k = (x_k, y_k, z_k) = [x_k \quad y_k \quad z_k]^t$ where x_k, y_k and z_k are unknown. First of all, in order to get an expression to be able to calculate x_k, y_k and z_k, a projection is done of the position vector, $\bar{r}_k$, on the vector of travel, $\bar{s}_{ik}$:

$$\bar{s}_{ik} \cdot \bar{r}_k = |\bar{s}_{ik}||\bar{r}_k| \cos\theta_{ik} \tag{32}$$

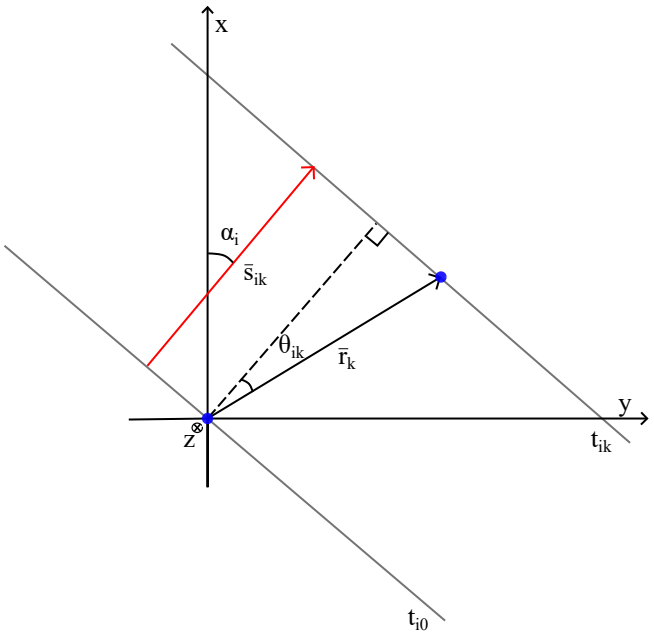

Figure 17: Geometry with a reference point at the origin and a sensor at position $\bar{r}_k$. The front of zero vertical electric field ($E_z = 0$) during run i passes the reference point at time t_{i0} and the sensor k at time t_{ik}. The vector of travel $\bar{s}_{ik}$ of the dipole is perpendicular to the fronts.

Both sides of Equation 32 are divided by $|\bar{s}_{ik}|$ which results in Equation 33.

$$\frac{\bar{s}_{ik}}{|\bar{s}_{ik}|} \cdot \bar{r}_k = |\bar{r}_k| \cos\theta_{ik} \tag{33}$$

It is known that the direction of $\bar{s}_{ik}$ is $(\cos\alpha_i, \sin\alpha_i, 0)$ and that $|\bar{r}_k| \cos\theta_{ik} = |\bar{s}_{ik}| = s_{ik}$ which gives Equation 34:

$$(\cos\alpha_i, \sin\alpha_i, 0) \cdot (x_k, y_k, z_k) = s_{ik} \tag{34}$$

Calculating the scalar product results in Equation 35.

$$x_k \cos\alpha_i + y_k \sin\alpha_i + 0 = s_{ik} \tag{35}$$

In Equation 35 both α_i and s_{ik} are known, as opposed to the position vector components x_k, y_k and z_k, which are unknown. In order to solve for x_k, y_k and z_k a system of equations is set up which needs to consist of at least two intersecting runs over the sensor group together with information about the depth of where the sensors are located. With the aim to set up the system of equations accurately an algorithm has been developed, where the first part of the algorithm consists of the following five steps.

I. Evaluate coefficients for each run.

II. Add equations for depth, z_k.

III. Check if runs are along coordinate axis. (optional)

IV. Determine number of linearly independent equations.

V. Solve system of equations for sensor coordinates.

Step I filters the data, removes possible offsets, selects a relevant interval and finds the zero crossings. After that the data points are converted to the relative time between the sensor and the reference point, τ_{ik}, and with that information, together with the input data about speed and course, the distance s_{ik} is calculated. Following, a matrix, A, where each row of the matrix represents one run, and one column-vector, b, where each value represents the distance s_{ik} for that run i, is created for each sensor k.

$$A\bar{r}_k = b \tag{36}$$

$$\begin{bmatrix} \cos\alpha_1 & \sin\alpha_1 & 0 \\ \cos\alpha_2 & \sin\alpha_2 & 0 \end{bmatrix} \begin{bmatrix} x_k \\ y_k \\ z_k \end{bmatrix} = \begin{bmatrix} s_{1k} \\ s_{2k} \end{bmatrix} \tag{37}$$

Since we are only measuring in the x-y-plane the coefficients of z_k will always be zero, however z_k is the depth of where the sensor is located and should therefore have a value. Step II gives z_k this value by adding a row to matrix A with coefficient 1 in the third column, as well as adding one value to vector b which equals to the depth of the sensor, i.e. the *a priori* depth value z_{apk}.

$$\begin{bmatrix} \cos\alpha_1 & \sin\alpha_1 & 0 \\ \cos\alpha_2 & \sin\alpha_2 & 0 \\ 0 & 0 & 1 \end{bmatrix} \begin{bmatrix} x_k \\ y_k \\ z_k \end{bmatrix} = \begin{bmatrix} s_{1k} \\ s_{2k} \\ z_{apk} \end{bmatrix} \tag{38}$$

If all runs over the sensor group are along only one of the coordinate axes, possibly with course and reverse course, it is only possible to get information about the sensors' position along that axis. Consequently that will not give any information about distances in the other axis's direction. To be able to solve the equation system in this case, step III checks each column in matrix A. If the magnitude of all elements of the column are equal to or less than machine epsilon it means that there is no information along the corresponding axis. An extra row is added to A with a 1 assigned in the present column, all other elements being 0. Correspondingly, a 0 is added to the same row in b. As an explicit example, if there are two runs along the y-axis with course 90° and 270°, as in Figure 18, we will only be able to get information about the sensors' location in y-direction and not in x-direction, therefore a 1 is inserted in the first column which is followed by zeros in the rest of the row, together with a zero in vector b as in Equation 39.

$$\begin{bmatrix} 0 & 1 & 0 \\ 0 & -1 & 0 \\ 0 & 0 & 1 \\ 1 & 0 & 0 \end{bmatrix} \begin{bmatrix} x_k \\ y_k \\ z_k \end{bmatrix} = \begin{bmatrix} s_{1k} \\ s_{2k} \\ z_{apk} \\ 0 \end{bmatrix} \tag{39}$$

To be able to solve the system of equations there has to be at least three linearly independent equations. Step IV calculates the rank of matrix A for each sensor and aborts the algorithm if the rank is less than 3, since the system of equations lacks a solution. Step V solves the system of equations in the least-squares-sense, since the system might be over-determined. This yields an estimate of the position vector $\bar{r}_k = (x_k, y_k, z_k)$ of each sensor.

3.1.1 *Error propagation and estimation*

The second part of the algorithm concerns error propagation. Measurement errors might occur in the course and speed of the dipole, which means that the error estimation of x_k, y_k and z_k depends

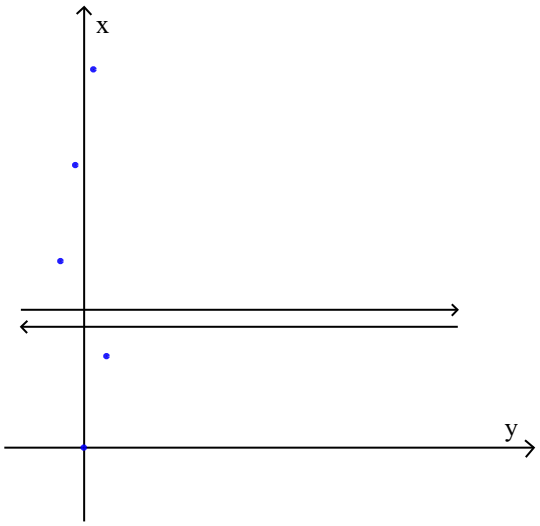

Figure 18: Two runs along coordinate axis y with opposing courses, 90° and 270°, which provide information about the sensors' locations in y-direction but not in x-direction.

on the course, α_i, and speed, v_i, of each run i. The position coordinates depend on the uncertain parameters of N runs in the following way $x_k = x_k(\alpha_1, \ldots, \alpha_N, v_1, \ldots, v_N)$, $y_k = y_k(\alpha_1, \ldots, \alpha_N, v_1, \ldots, v_N)$, $z_k = z_k(\alpha_1, \ldots, \alpha_N, v_1, \ldots, v_N)$.

To calculate the error estimation Δx_k, Δy_k and Δz_k to linear order the partial derivative of each run ($i = 1, \ldots, N$) with respect to course, α_i, and speed, v_i, is multiplied with $\Delta\alpha_i$ and Δv_i for the corresponding run respectively as in Equation 40 – Equation 42.

$$\Delta x_k \approx \Delta\alpha_1 \frac{\partial x_k}{\partial \alpha_1} + \Delta v_1 \frac{\partial x_k}{\partial v_1} + \cdots + \Delta\alpha_N \frac{\partial x_k}{\partial \alpha_N} + \Delta v_N \frac{\partial x_k}{\partial v_N} \tag{40}$$

$$\Delta y_k \approx \Delta\alpha_1 \frac{\partial y_k}{\partial \alpha_1} + \Delta v_1 \frac{\partial y_k}{\partial v_1} + \cdots + \Delta\alpha_N \frac{\partial y_k}{\partial \alpha_N} + \Delta v_N \frac{\partial y_k}{\partial v_N} \tag{41}$$

$$\Delta z_k \approx \Delta\alpha_1 \frac{\partial z_k}{\partial \alpha_1} + \Delta v_1 \frac{\partial z_k}{\partial v_1} + \cdots + \Delta\alpha_N \frac{\partial z_k}{\partial \alpha_N} + \Delta v_N \frac{\partial z_k}{\partial v_N} \tag{42}$$

In general, the values of $\Delta\alpha_i$ and Δv_i should be provided together with α_i and v_i. Lacking that, the approximations $\pm$ 5° and $\pm$ 0.5 kn are used respectively. All partial derivatives needs to be calculated. This can be done by creating a system of equations through implicit differentiation. Calculating the partial derivative of Equation 38 with respect to α_i results in Equation 43 and Equation 44.

$$\cos\alpha_i \cdot \frac{\partial x_k}{\partial \alpha_i} + \sin\alpha_i \cdot \frac{\partial y_k}{\partial \alpha_i} = x_k \sin\alpha_i - y_k \cos\alpha_i \tag{43}$$

$$1 \cdot \frac{\partial z_k}{\partial \alpha_i} = 0 \tag{44}$$

Calculating the partial derivative of Equation 38 with respect to v_i on the other hand leads to Equation 45 and Equation 46.

$$\cos \alpha_i \cdot \frac{\partial x_k}{\partial v_i} + \sin \alpha_i \cdot \frac{\partial y_k}{\partial v_i} = \tau_{ik} \tag{45}$$

$$1 \cdot \frac{\partial z_k}{\partial v_i} = 0 \tag{46}$$

Accordingly the system of equations turns out as Equation 47, providing that the input data still consists of two runs, 1 and 2. Note that the coefficient matrix is identical to that in Equation 38, and the right hand side contains non-zero entries corresponding to the runs. The implicit differential scheme will result in an analogous system when step III of the main algorithm is activated, i.e. when applied to an equation similar to Equation 39.

$$\begin{bmatrix} \cos\alpha_1 & \sin\alpha_1 & 0 \\ \cos\alpha_2 & \sin\alpha_2 & 0 \\ 0 & 0 & 1 \end{bmatrix} \begin{bmatrix} \frac{\partial x_k}{\partial \alpha_1} & \frac{\partial x_k}{\partial v_1} & \frac{\partial x_k}{\partial \alpha_2} & \frac{\partial x_k}{\partial v_2} \\ \frac{\partial y_k}{\partial \alpha_1} & \frac{\partial y_k}{\partial v_1} & \frac{\partial y_k}{\partial \alpha_2} & \frac{\partial y_k}{\partial v_2} \\ \frac{\partial z_k}{\partial \alpha_1} & \frac{\partial z_k}{\partial v_1} & \frac{\partial z_k}{\partial \alpha_2} & \frac{\partial z_k}{\partial v_2} \end{bmatrix} = \tag{47}$$

$$\begin{bmatrix} x_k \sin\alpha_1 - y_k \cos\alpha_1 & \tau_{1k} & 0 & 0 \\ 0 & 0 & x_k \sin\alpha_2 - y_k \cos\alpha_2 & \tau_{2k} \\ 0 & 0 & 0 & 0 \end{bmatrix}$$

The system of equations is solved in the least-squares-sense to obtain the values of the partial derivatives. Consequently, Δx_k, Δy_k and Δz_k are calculated by substituting all obtained values in Equation 40 – Equation 42.

A more conservative estimate is obtained by applying the triangle inequality to Equation 40 – Equation 42, resulting in:

$$\Delta x_k \leqslant \sum_{i=1}^{N} (|\Delta\alpha_i| \cdot |\frac{\partial x_k}{\partial \alpha_i}| + |\Delta v_i| \cdot |\frac{\partial x_k}{\partial v_i}|) \tag{48}$$

$$\Delta y_k \leqslant \sum_{i=1}^{N} (|\Delta\alpha_i| \cdot |\frac{\partial y_k}{\partial \alpha_i}| + |\Delta v_i| \cdot |\frac{\partial y_k}{\partial v_i}|) \tag{49}$$

$$\Delta z_k \leqslant \sum_{i=1}^{N} (|\Delta\alpha_i| \cdot |\frac{\partial z_k}{\partial \alpha_i}| + |\Delta v_i| \cdot |\frac{\partial z_k}{\partial v_i}|). \tag{50}$$

4

RESULTS

The algorithm results in an estimate of the position vector $\bar{r}_k = (x_k, y_k, z_k)$ as well as an error estimation. The data files that are used in the algorithm to get the result in Table 1 – Table 3 are called 'LV4a' and 'LV4b' created in 2012 by the Swedish Defence Research Agency. The first file 'LV4a' consist of measurement data on course 270° and the second one 'LV4b' consists of measurement data on course 90°, both with speed 5 kn and sensor depth 9.6 m. That means that they are on course and reverse course to each other, both along the y-axis. Due to that we will only be able to get information about each sensor's location in y-direction, y_k. The sensors are located at the x-axis in a straight line mounted on a beam at $y_k = 0$ m with approximate spacing 5 m in x-direction, giving that the sensors' location are known before hand. The predicted location in Table 1, Table 2 and Table 3 can therefore easily be compared with the known location. The predictions are calculated using data file 'LV4a' and 'LV4b' alone as well as data from both files combined named 'LV4a' & 'LV4b' in the tables. Unfortunately, data for sensor 5 is missing and therefore no results for sensor 5 can be displayed.

Table 1: Predicted relative position in y-direction from the reference point (sensor 2) to sensor 1 – 4 obtained from the algorithm presented in Section 3.1.

data file	y_1	y_2	y_3	y_4
'LV4a'	0.036	0	-0.244	-0.112
'LV4b'	-0.337	0	-0.028	0.221
'LV4a' & 'LV4b'	-0.151	0	-0.136	0.055

Table 2: Error estimation of the sensors' position depending on speed and course with the approximate uncertainty $\Delta v = \pm 0.5$ kn and $\Delta\alpha = \pm 5°$.

data file	Δy_1	Δy_2	Δy_3	Δy_4
'LV4a'	0.007	0	-0.048	-0.022
'LV4b'	-0.066	0	-0.005	0.043
'LV4a' & 'LV4b'	-0.030	0	-0.027	0.011

Table 3: Error estimation with applied triangle inequality of the sensors' position depending on speed and course with the approximate uncertainty $\Delta v = \pm 0.5$ kn and $\Delta\alpha = \pm 5°$.

data file	$\lvert\Delta y_1\rvert$	$\lvert\Delta y_2\rvert$	$\lvert\Delta y_3\rvert$	$\lvert\Delta y_4\rvert$
'LV4a'	0.007	0	0.048	0.022
'LV4b'	0.066	0	0.005	0.043
'LV4a' & 'LV4b'	0.037	0	0.027	0.033

Compared to hydro-acoustic methods presented in Section 2.3 this result is within about 0.2 m from the actual position while hydro-acoustic methods often get a result within a couple of centimetres or decimetres depending on e.g. depth. A hydro-acoustic method might be better to some extent but the result is within the same order of magnitude.

The result of how the prediction of the sensors' location is affected by an uneven dipole, described in Section 2.2.2, is presented in Table 4 – Table 6 and Table 7 – Table 9. Simulated data have been used where the two sources are placed at depth 1 m and 2 m on the course line for a non-horizontal dipole, and at depth 2 m but with an 0.5 m offset from the course line for one of the dipole sources. The speed was set to 5 kn and sensor depth to 10 m. The prediction for each case is based on two different simulated runs over the sensor group, 'syntest1' and 'syntest2' for non-horizontal dipole and 'syntest3' and 'syntest4' for a dipole with sideways offset, which are on course 0° and 180° respectively along the x-axis. Consequently the position will only be obtained in x-direction, x_k. The prediction is made on 'syntest1', 'syntest2', 'syntest3' and 'syntest4' separately as well as 'syntest1' combined with 'syntest2' and 'syntest3' combined with 'syntest4'.

As seen from the field image in Figure 11 in Section 2.2.2.1 the zero crossings are curved when the dipole is non-horizontal, which also can be observed from the result in Table 4 – Table 6 since the predicted value is either positive or negative for the sensor in the middle and of opposite sign for the sensors at the edges. Further, as seen from

Table 4: Predicted relative position in x-direction from the reference point (sensor 2) to sensor 1 – 5 obtained from the algorithm presented in Section 3.1 when the dipole is non-horizontal.

data file	x_1	x_2	x_3	x_4	x_5
'syntest1'	0.241	0	-0.077	0.000	0.241
'syntest2'	-0.241	0	0.077	0.000	-0.241
'syntest1' & 'syntest2'	0.000	0	0.000	0.000	0.000

Table 5: Error estimation of the sensors' position depending on speed and course with the approximate uncertainty $\Delta v = \pm 0.5$ kn and $\Delta\alpha = \pm 5°$ when the dipole is non-horizontal.

data file	Δx_1	Δx_2	Δx_3	Δx_4	Δx_5
'syntest1'	0.047	0	-0.015	0.000	0.047
'syntest2'	-0.047	0	0.015	0.000	-0.047
'syntest1' & 'syntest2'	0.000	0	0.000	0.000	0.000

Table 6: Error estimation with applied triangle inequality of the sensors' position depending on speed and course with the approximate uncertainty $\Delta v = \pm 0.5$ kn and $\Delta\alpha = \pm 5°$ when the dipole is non-horizontal.

data file	$\lvert\Delta x_1\rvert$	$\lvert\Delta x_2\rvert$	$\lvert\Delta x_3\rvert$	$\lvert\Delta x_4\rvert$	$\lvert\Delta x_5\rvert$
'syntest1'	0.047	0	0.015	0.000	0.047
'syntest2'	0.047	0	0.015	0.000	0.047
'syntest1' & 'syntest2'	0.047	0	0.015	0.000	0.047

Table 7: Predicted relative position in x-direction from the reference point (sensor 2) to sensor 1 – 5 obtained from the algorithm presented in Section 3.1 when the front source of the dipole is offset sideways from the source line by 0.5 m.

data file	x_1	x_2	x_3	x_4	x_5
'syntest3'	-0.147	0	0.199	0.399	0.551
'syntest4'	0.147	0	-0.199	-0.399	-0.551
'syntest3' & 'syntest4'	0.000	0	0.000	0.000	0.000

Table 8: Error estimation of the sensors' position depending on speed and course with the approximate uncertainty $\Delta v = \pm 0.5$ kn and $\Delta\alpha = \pm 5°$ when the front source of the dipole is offset sideways from the source line by 0.5 m.

data file	Δx_1	Δx_2	Δx_3	Δx_4	Δx_5
'syntest3'	-0.029	0	0.039	0.078	0.108
'syntest4'	0.029	0	-0.039	-0.078	-0.108
'syntest3' & 'syntest4'	0.000	0	0.000	0.000	0.000

Table 9: Error estimation with applied triangle inequality of the sensors' position depending on speed and course with the approximate uncertainty $\Delta v = \pm 0.5$ kn and $\Delta\alpha = \pm 5°$ when the front source of the dipole is offset sideways from the source line by 0.5 m.

data file	$\lvert\Delta x_1\rvert$	$\lvert\Delta x_2\rvert$	$\lvert\Delta x_3\rvert$	$\lvert\Delta x_4\rvert$	$\lvert\Delta x_5\rvert$
'syntest3'	0.029	0	0.039	0.078	0.108
'syntest4'	0.029	0	0.039	0.078	0.108
'syntest3' & 'syntest4'	0.029	0	0.039	0.078	0.108

the field images in Figure 12 and Figure 13 in Section 2.2.2.1 the zero crossings are shifted when the front source is offset from the course line which can be seen from the result in Table 7 – Table 9 since the predicted value is negative for the sensor at one end and positive for the sensor at the other end and vice versa.

The result of how the prediction of the sensors' location is affected by a tilted sensor is presented in Table 10 – Table 12 and Table 13 – Table 15. The data used is two simulated runs over the sensor group, 'rot1' and 'rot2', which are on course 0° and 180° respectively along the x-axis. The electric field for sensor 5 is multiplied with the rotation matrix for yaw, pitch and roll presented in Section 2.2.4. However the angle for yaw and roll, designated α and γ, is set to zero while the angle for pitch, designated γ, is set to 10° respectively 1° meaning that the sensors coordinate system is rotated around the y-axis. The prediction is based on data for 'rot1' and 'rot2' with pitch angle 10° as well as 1° both separately and together named 'rot1' & 'rot2' in the tables.

Table 10: Predicted relative position in x-direction from the reference point (sensor 2) to sensor 1 – 5 obtained from the algorithm presented in Section 3.1 when sensor 5 is tilted 10° around the y-axis.

data file	x_1	x_2	x_3	x_4	x_5
'rot1'	0.000	0	0.000	0.000	-1.772
'rot2'	0.000	0	0.000	0.000	-1.772
'rot1' & 'rot2'	0.000	0	0.000	0.000	-1.772

Table 11: Error estimation of the sensors' position depending on speed and course with the approximate uncertainty $\Delta v = \pm 0.5$ kn and $\Delta\alpha = \pm 5°$ when sensor 5 is tilted 10° around the y-axis.

data file	Δx_1	Δx_2	Δx_3	Δx_4	Δx_5
'rot1'	0.000	0	0.000	0.000	-0.347
'rot2'	0.000	0	0.000	0.000	-0.347
'rot1' & 'rot2'	0.000	0	0.000	0.000	-0.347

Table 12: Error estimation with applied triangle inequality of the sensors' position depending on speed and course with the approximate uncertainty $\Delta v = \pm 0.5$ kn and $\Delta\alpha = \pm 5°$ when sensor 5 is tilted 10° around the y-axis.

data file	$\lvert\Delta x_1\rvert$	$\lvert\Delta x_2\rvert$	$\lvert\Delta x_3\rvert$	$\lvert\Delta x_4\rvert$	$\lvert\Delta x_5\rvert$
'rot1'	0.000	0	0.000	0.000	0.347
'rot2'	0.000	0	0.000	0.000	0.347
'rot1' & 'rot2'	0.000	0	0.000	0.000	0.347

Table 13: Predicted relative position in x-direction from the reference point (sensor 2) to sensor 1 – 5 obtained from the algorithm presented in Section 3.1 when sensor 5 is tilted 1° around the y-axis.

data file	x_1	x_2	x_3	x_4	x_5
'rot1'	0.000	0	0.000	0.000	-0.181
'rot2'	0.000	0	0.000	0.000	-0.181
'rot1' & 'rot2'	0.000	0	0.000	0.000	-0.181

Table 14: Error estimation of the sensors' position depending on speed and course with the approximate uncertainty $\Delta v = \pm 0.5$ kn and $\Delta\alpha = \pm 5°$ when sensor 5 is tilted 1° around the y-axis.

data file	Δx_1	Δx_2	Δx_3	Δx_4	Δx_5
'rot1'	0.000	0	0.000	0.000	-0.036
'rot2'	0.000	0	0.000	0.000	-0.036
'rot1' & 'rot2'	0.000	0	0.000	0.000	-0.036

Table 15: Error estimation with applied triangle inequality of the sensors' position depending on speed and course with the approximate uncertainty $\Delta v = \pm 0.5$ kn and $\Delta\alpha = \pm 5°$ when sensor 5 is tilted 1 $^{\mathrm{circ}}$ around the y-axis

data file	$\lvert\Delta x_1\rvert$	$\lvert\Delta x_2\rvert$	$\lvert\Delta x_3\rvert$	$\lvert\Delta x_4\rvert$	$\lvert\Delta x_5\rvert$
'rot1'	0.000	0	0.000	0.000	0.036
'rot2'	0.000	0	0.000	0.000	0.036
'rot1' & 'rot2'	0.000	0	0.000	0.000	0.036

5 DISCUSSION

From the result in Table 1 – Table 3 it is observed that the prediction becomes better when data from different runs are combined. The predictions of the position for all sensors are then within 0.2 m from the actual position, however the error estimation shows that there should only be a difference between calculated and actual position of a couple of centimetres. Consequently the predicted result must depend on other factors than speed and course of the vessel, since the error estimation does not contribute with the dominating error.

Both a non-horizontal dipole and a dipole where one of the sources are offset sideways from the course line could be crucial to the measurement and could therefore be a reason for the error. To investigate this a simulated data file discussed in Section 2.2.2 with a non-horizontal dipole in the first case, and a dipole source with offset from the course line in the second case, was used at course and reverse course. The prediction is presented in the result in Table 4 – Table 6 and what can be seen is that the error an uneven dipole entails contributes to the error of the predicted location if data from only one run over the sensor group is used, nevertheless it does not contribute to the error if data from two runs over the sensor group is used at course and reverse course to each other since the error in that case gets cancelled out.

Further, it is probable that the result of the predictions depend on the sensors alignment in the coordinate system, if a sensor isn't aligned correctly but is tilted an error might occur. Simulated data on course and reverse course was used to investigate the case and as noticed from the result in Table 7 – Table 9 the predicted value for the sensors' position is the same for the both runs. This indicates that a tilted sensor gives a systematic displacement in the position determination, meaning the error a systematic displacement brings does not cancel when processing data at course and reverse course. In addition, the suggested algorithm seems quite sensitive to sensor rotation, since a pitch angle of only 1° results in a position error of almost 0.2 m for the considered parameters. This is of the same order of magnitude as the observed deviations when processing real experimental data.

The impact of a sloping seabed could be another reason for error in the result. The current from the dipole is affected by the high contrast at the water-seabed-interface and instead of flowing freely from the source the current swerves close to the seabed and travels along the bottom. Consequently the electric field from the dipole follows the

curvature of the bottom of the sea. Since the sensors are located just above the seabed this means that the electric field emitted from the dipole is affected around the sensors and the zero crossings of the z-components of the electric field might be dislocated. This would affect the result since the algorithm to do the prediction is based on the zero crossings of the z-components. A possible way to evaluate this mathematically is by calculating the case with 3D-codes, however that is not within the scope of this master thesis.

The possible stated sources of error seem likely regarding their order of magnitude. For errors that tend to cancel each other out on course and reverse course, it will be advantageous to process several pairs of runs in order to obtain a more stable and accurate position estimate from the resulting average value. As presented in the result, a hydro-acoustic method might be better but the two methods are still within the same order of magnitude which is a promising result. Even though an acoustic method would bring a slightly better result the advantage of not having to use an external acoustic sensor when confirming the sensors' location could be significant, due to a less complex measurement set-up which reduces the risk of errors.

6

SUMMARY AND CONCLUSIONS

The answer to the first question in the beginning of the thesis, whether it is possible to position electric field underwater sensors with the sensor system itself, is yes it is possible. With the second question, asking how accurate the estimated position of the sensors are, the answer gets a bit more complex. The predicted result from experimental data with 10 m sensor depth is within 0.2 m from the actual position while the error estimation is within a couple of centimetres, indicating that the error must depend on something more than speed and course which the error estimation is calculated upon. Conceivable sources of error are the impact of a non-horizontal dipole, a dipole with a source offset sideways, a tilted sensor as well as a sloping seabed. A non-horizontal dipole contributes with an error of a couple of decimetres, nevertheless the error is cancelled out if data is used at course and reverse course to each other. The same is for a dipole where one of the sources are offset sideways which also contributes with an error of a couple of decimetres but which is cancelled out at course and reverse course. Consequently, it would be advantageous to process several pairs of runs over the sensor group in order to obtain a more stable and accurate position. A tilted sensor gives a systematic error from up to more than a metre to a couple of centimetres depending on how much the sensor is tilted, indicating that the algorithm is quite sensitive for sensor rotation. Additionally, data used on course and reverse course does not compensate for this error. Lastly, a sloping seabed might affect the predicted result by making the electric field follow the curvature of the bottom, hence affecting the zero crossings of the z-components. The accuracy of the estimated position is acceptable but could be better if the error of an uneven dipole, tilted sensor and sloping seabed was taken into account in the algorithm. The answer to the third question, whether the method using the sensor system itself is better than hydro-acoustic methods, is no. Having that said it is not much worse either, they are within the same order of magnitude. A clear advantage of using the sensor system itself is that an external acoustic sensor is not needed when verifying the position of the electric sensors. In conclusion, the method has acceptable performance to verify the position of electric underwater sensors.

BIBLIOGRAPHY

[1] Qiang Bai and Yong Bai. *Subsea Pipeline Design, Analysis and Installation*. 1st ed. Texas, USA: Gulf Professional Publishing - Elsevier, 2014, pp. 487–509.

[2] Dr. Patrizio Di Benedetto-Archaeologist, Mr. Digiugno Calcedonio Daniele-Mining Surveyor, Mr. Liggieri Sebastiano Giovanni-Surveyor, and Mr. Spadaro Andrea-Surveyor. "Underwater Acoustic Positioning System." In: *The Academy of Marine Positioning Bathymetry* (2012), pp. 7–8.

[3] David K. Cheng. *Field and Wave Electromagnetics*. 2nd ed. London, England: Addison-Wesley, 1989.

[4] Lennart Crona and Anders Brage. "Carbon Fibre Electrodes and their Qualities in Salt Water." In: *International Conference on Marine Electromagnetics* FOA-B–98-00319–SE (1997), pp. 1–5.

[5] Jonathan C. Crowell. "Underwater Acoustic Positioning System and Method." In: *United States Patent* US 8,009,516 B2 (2011), pp. 1–2.

[6] Herbert Goldstein. *Classical Mechanics*. 2nd ed. Boston, USA: Addison-Wesley, 1980.

[7] *HiPAP - Acoustic Underwater Positioning and Navigation Systems*. HiPAP models overview. Kongsberg. 2020.

[8] *Mini-Ranger 2 USBL - Underwater Target Tracking and Communications*. Why Mini-Ranger 2 USBL. Sonardyne. 2020.

[9] Håkan Nilsson. "Hydroakustisk kommunikation, nya förmågor i Marinen?" PhD thesis. Stockholm, Sverige, 2002, pp. 11–17.

[10] Elaine Rowan. "LBL Underwater Positioning." In: *Hydro International* (2008), pp. 1–2.

[11] *Subsonus USBL/INS*. Datasheet. Advanced navigation. 2020.

[12] Donald Thomson. "Acoustic Positioning Systems." In: *Hydrofest* (2005), p. 26.

[13] Keith Vickery. "Acoustic Positioning Systems "A Practical Overview Of Current Systems"." In: *Proceedings of the 1998 Workshop on Autonomous Underwater Vehicles* (1998), pp. 2–6.

[14] Olov Ågren. *Elektromagnetism*. 1st ed. Lund, Sverige: Studentlitteratur, 2014.

COLOPHON

This thesis work was conducted by Maria Langkilde in collaboration with the Swedish Defence Research Agency in Stockholm, Kista.

LaTeXtemplate adapted from https://bitbucket.org/amiede/classicthesis/.

Final Version as of January 28, 2021.